Diffusion Tensor MR Imaging

OVERVIEW

Theoretical description of the motion of spins depends heavily on the nature of motion and its relevance to specifics of the MRI (magnetic resonance imaging) procedure. In Chapter B1, for example, the equation of motion relates to the precession of spin magnetization in response to constant and time-varying magnetic fields. In terms of localization concepts outlined in Chapter B4, there is an implicit assumption of motionless spins to simplify treatments of spatial encoding. For Chapter B7, on the other hand, the formalism is explicitly developed to address the translational movement of spins through gradient fields. Macroscopic motion of this sort during an imaging sequence can lead to phase and/or amplitude effects that either manifest as artifact, or are harnessed in specialized sequences to visualize flow and kinetics. Within the context of "diffusion," however, the scale and nature of motions are quite distinct from those discussed thus far. Additionally, diffusion is a physical process totally independent of magnetization and resonance concepts. That said, NMR (nuclear magnetic resonance) is recognized as the preferred means to noninvasively document molecular diffusion phenomena. Of great practical importance to the MRI community, diffusion-sensitive sequences are readily incorporated into imaging sequences to derive diffusion-based contrast of tissues in vivo. Diffusion-weighted contrast is used extensively as a diagnostic screen for acute stroke in the brain, but this only marks the beginning of diffusion information available to clinicians. As outlined in *UNIT A6.4*, the directional dependence of diffusion (i.e., diffusion anisotropy) may be exploited to visualize cellular order in white matter, as well as disease processes that infiltrate and undermine this structural order. The physical principles and methodologies involved in diffusion-weighted imaging (DWI) and diffusion tensor imaging (DTI) are summarized in this unit.

Diffusion imaging targets the random molecular motion of water in tissue. Molecular diffusion within and among cells is recognized as a rather complex process that is dependent on many factors. Several of the main factors include cell size and density, water permeability between intracellular and extracellular spaces, and water interaction with macromolecules. Consequently, MR images that accentuate diffusion-dependent contrast provide indirect insight into these cellular properties.

Additional gradient pulses incorporated within the imaging sequence are used to elicit diffusion contrast. Typically diffusion-gradient pulses are strong (i.e., near full strength) and long (tens of milliseconds) relative to those used in routine imaging. Such gradient pulses impart strong phase shifts to water molecules dependent on their microscopic translational trajectories. The more mobile the water is, the greater the spread in phase shifts, thus the greater degree of signal loss due to the spin dephasing. Diffusion sensitivity of an imaging sequence is determined by the operator-controlled parameter called "*b*-factor." Analogous to T_E in T_2-weighting, an increase in the *b*-factor increases diffusion-weighted contrast. However, one should be aware of potentially confusing nomenclature used to describe diffusion. As implied above, unrestricted water, such as in CSF (cerebrospinal fluid), is highly mobile and will dephase to yield low signal intensity on heavily diffusion-weighted images. Conversely, severely restricted water, e.g., within cellular dense tissues, exhibits relatively strong signal on DWI. Thus, the contrast on DWI is often reversed relative to conventional T_2-weighted contrast. Images acquired at multiple diffusion sensitizations (i.e., *b*-factors) can be mathematically combined to produce an apparent diffusion coefficient (ADC) image wherein image intensity represents water mobility. Thus, an ADC image tends to resemble a conventional T_2-weighted image. Examples of these various image formats are illustrated in Figures B8.1.2 and B8.1.3.

Contributed by Thomas L. Chenevert and Robert C. Welsh

Current Protocols in Magnetic Resonance Imaging (2004) B8.1.1-B8.1.13

An important feature of water movement in tissue is that diffusion may be anisotropic. That is, structural order and directionality translates to a directional dependence of water mobility. The greatest clinical example of this is high water mobility when measured parallel to white matter fiber tracts and low mobility perpendicular to the tracts. Substantial efforts in mathematical formalism, models, and techniques have been developed to describe and measure anisotropic diffusion in vivo. Fortunately, many of the technical impediments have been overcome such that anisotropic diffusion properties of the CNS (central nervous system) are now readily imaged in clinical applications. Diffusion tensor imaging is the most common approach to visualize diffusion in anisotropic tissues. The tensor is a mathematical extension of the single-valued diffusion coefficient and accounts for multiple diffusion values with direction. The multiplicity of diffusion values can be reduced to an average diffusion coefficient with respect to direction that is equivalent to the ADC. Several additional parameters have been devised to denote the strength of anisotropy. Two of the more popular include the fractional anisotropy (FA) and relative anisotropy (RA), which are defined to exhibit areas of highly directional tissues, such as white matter in the corpus callosum, as bright areas on anisotropy (FA or RA) maps. Lastly, the actual direction of greatest water mobility can be derived from diffusion tensor data in each imaged voxel. The direction of the greatest water mobility is then represented by a two-dimensional fiber plot or directionally encoded color map which augments the FA or RA map. These representations are designed to give the reader a sense of fiber "grain" and connectivity. Fiber "tractography" is an extreme extension of these concepts and represents a promising area of investigation. In overly simple terms, fiber tractography algorithms utilize information provided by DTI to derive probable continuity in fibers in three dimensions. The resultant synthetic 3-D images of white matter fiber tracts in the brain are visually impressive, but one should realize validation of these approaches is still under investigation.

TECHNICAL DISCUSSION

Basic Diffusion Formalism

Molecular diffusion refers to the thermally driven random translational motion of molecules in media. Diffusion is also referred to as Brownian motion where media viscosity, temperature and the molecular mass are key aspects that determine mobility. In terms of MRI, it is the mobility of water molecules within tissue that is of interest. Unlike relaxation, T_1 and T_2, that have complex dependencies on translational and rotational motions of the spins which interact with the lattice via magnetic fields, diffusion is purely translational and is not considered an NMR process. That is, molecular diffusion occurs independent of magnetic fields and moments. Nevertheless, NMR provides the means to probe diffusion processes with excellent fidelity.

We begin with the Bloch equation, initially presented in *UNIT B3.1*. Equation B3.1.20 is modified with an additional term to become the Bloch-Torrey equation, which accounts for diffusion as follows:

$$\frac{d\vec{M}}{dt} = \gamma\vec{M} \times \vec{B}_{ext} + \frac{1}{T_1}\left(M_0 - M_z\right)\hat{z} - \frac{1}{T_2}\vec{M}_\perp + D\nabla^2\vec{M}_\perp \qquad \textbf{(B8.1.1)}$$

where D represents the diffusion coefficient in units of mm^2/sec (see *UNIT B3.1* for definition of other variables). As is often done, one simplifies the situation by considering the system in the rotating frame of reference (see *UNIT B1.2*) and assuming that any incremental field is provided by a linear field gradient (see *UNIT B4.1*) such that $\vec{B}_{\text{ext}}\hat{z} \rightarrow \vec{G} \bullet \vec{r}\hat{z}$.Consistent with discussion in *UNITS B4.1 & B7.1*, spins in a gradient field accumulate phase in proportion

to the gradient strength, duration, and position along the gradient. However, this concept is generalized for time-dependent position and gradient waveforms as:

$$\phi(t') = -\gamma \int_0^t \vec{G}(t') \bullet \vec{r}(t') dt' \qquad \textbf{(B8.1.2)}$$

For the scenario of a large number of spins exhibiting random motion trajectories, it can be shown that the net phase shift averaged over all spins is zero. Given this, one can pose the solution to Equation B8.1.1 for the transverse magnetization, $\vec{M}_\perp$, to include a diffusion-dependent factor that only affects amplitude, as:

$$\vec{M}_\perp(\vec{r},t) = \vec{M}_\perp^{D=0}(\vec{r},t) \cdot A(t) \qquad \textbf{(B8.1.3)}$$

where $\vec{M}_\perp^{D=0}(\vec{r},t)$ is the solution to the Bloch-Torrey equation in the absence of diffusion, and *A(t)* incorporates any time-dependent amplitude effect of diffusion. The solution to the diffusionless Bloch equation is known:

$$\vec{M}_\perp^{D=0}(\vec{r},t) = \vec{M}_\perp(\vec{r},0) e^{-t/T_2} e^{-i\gamma \vec{r} \bullet \int_0^t \vec{G}(t')dt'} \qquad \textbf{(B8.1.4)}$$

Consistent with formalism in *UNITS B3.1 & B4.1*, this solution includes T_2 relaxation and a phase dependence on position in the gradient field. From this point, standard procedures to substitute Equations B8.1.3 and B8.1.4 into B8.1.1, then eliminate common terms, will yield an ordinary differential equation for *A(t)* assuming $\vec{M}_\perp(\vec{r},0)$ is a constant:

$$\frac{1}{A}\frac{dA}{dt} = -D\vec{k}(t) \bullet \vec{k}(t)$$

where

$$\vec{k}(t) = \gamma \int_0^t \vec{G}(t')dt' \qquad \textbf{(B8.1.5)}$$

Finally, this is readily solved to yield the diffusion-dependent factor, which modulates the amplitude of transverse magnetization of the NMR/MRI signal, as:

$$A(t) = A_0 e^{-D\int_0^t \vec{k}(t') \bullet \vec{k}(t')dt'} \qquad \textbf{(B8.1.6)}$$

Measures of Water Diffusion in Tissue

The integral within Equation B8.1.6 is commonly referred to as the "*b*-factor." In close analogy to how T_E controls T_2 sensitivity, the *b*-factor controls sensitivity of the MRI experiment to diffusion effects. For the simple bipolar gradient waveform (often referred to as Stejskal-Tanner diffusion gradient pair) illustrated in Figure B8.1.1, the *b*-factor is:

$$b = (\gamma G \delta)^2 \left[\Delta - \frac{\delta}{3}\right] \qquad \textbf{(B8.1.7)}$$

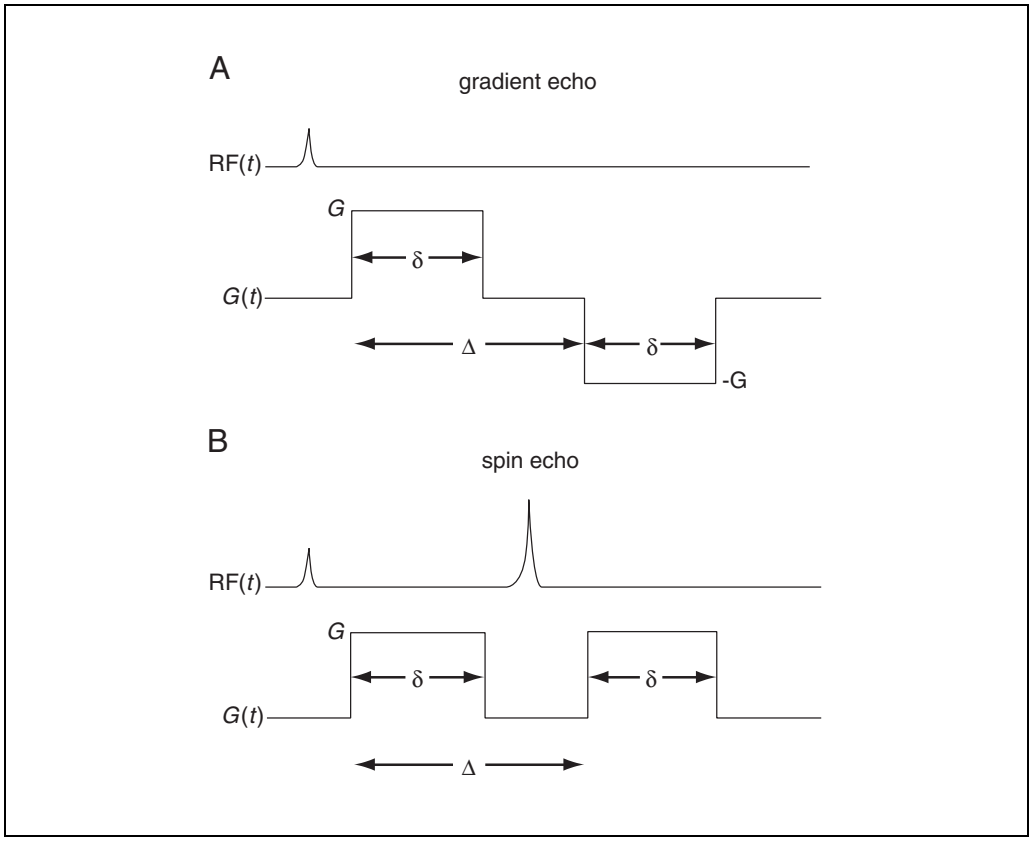

Figure B8.1.1 Bipolar gradient waveforms used to induce diffusion-dependent signal attenuation in (**A**) gradient echo or (**B**) spin echo sequences. Sensitivity to diffusion is controlled by the *b*-factor, given by $b = (\gamma G \delta)^2 [\Delta - (\delta/3)]$.

Typically, only the gradient amplitude is altered, leading to a change in signal amplitude, S_b, as a function of *b*-value. This directly leads to calculation of the diffusion coefficient via:

$$\ln\left(\frac{S_b}{S_0}\right) = -bD$$

or **(B8.1.8)**

$$D = -\frac{1}{(b_2 - b_1)}\ln\left(\frac{S_{b_2}}{S_{b_1}}\right)$$

where S_0 is the signal without diffusion gradients (i.e., $G = 0$). As graphically illustrated in Figure B8.1.2, *D* can be determined by a fitted slope of signal attenuation at multiple *b*-values or by the log-ratio of signals at two *b*-values.

One can also study diffusion effects as a function of evolution time, Δ. In a free diffusion environment where diffusing molecules do not encounter restrictive boundaries (e.g., simple fluid), the measured diffusion coefficient is independent of Δ. In tissue, however, the system is far more complex, with the mobility of water molecules hindered by macromolecules, cell membranes, and extracellular structures. Classic diffusion theory provides an estimate of the root-mean-square (rms) displacement of a freely diffusing molecule over the interval Δ to be $(2D\Delta)^{1/2}$ in any one direction, or $(6D\Delta)^{1/2}$ in three dimensions. Assuming a diffusion coefficient $D = 10^{-3}$ mm^2/sec and evolution time Δ =

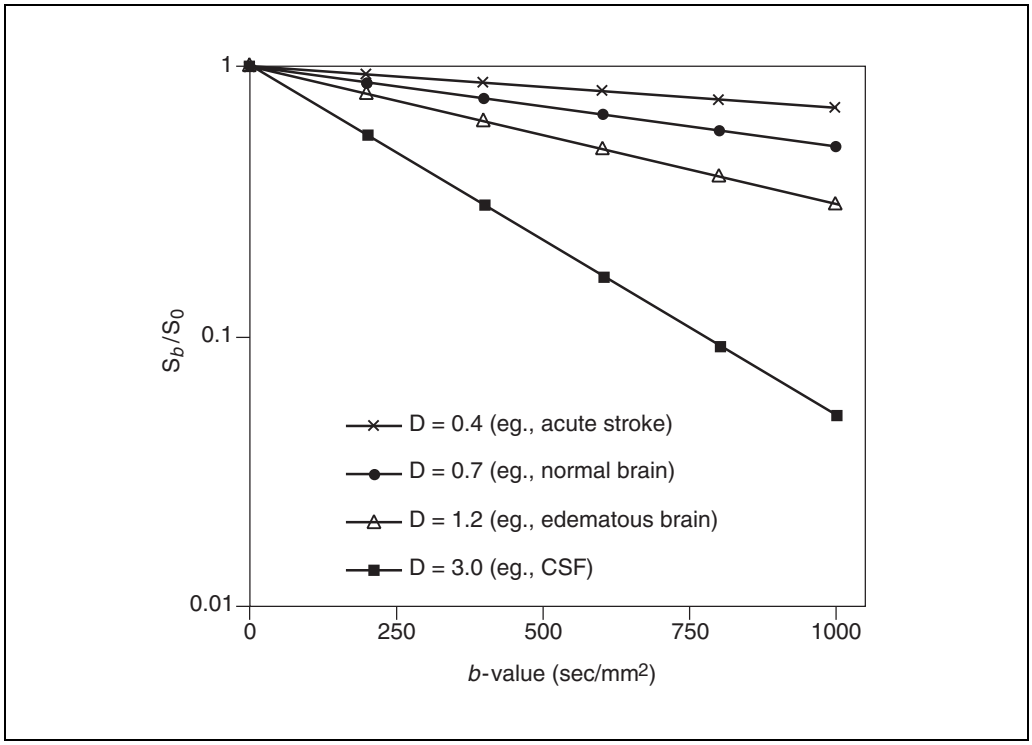

Figure B8.1.2 Simulated signal loss as a function of *b*-value based on representative tissue diffusion coefficients in units of 10^{-3} mm^2/sec.

50 msec, the rms displacement is 17 μm. Given that cellular dimensions are on the order of 1 to 10 μm and the majority of water in the brain tissue is intracellular, the probability that a water molecule will encounter semirestrictive cellular membranes over this interval is high. There are also active cellular transport, convective motion, flow in capillaries and larger vessels, and bulk tissue motions that contribute to increase the apparent mobility of water in vivo. These effects can lead to nonlinear behavior in $\ln(S_b/S_o)$ as a function of *b*-value and evolution time. In consideration of all of these complex influences, diffusion measurements in tissues are usually referred to with the qualifier "apparent" diffusion coefficient, or ADC.

Maximum gradient strength on clinical MRI systems is typically 20 to 40 mT/m, although greater effective strength can be achieved by simultaneous combination of *X*, *Y*, and *Z* gradients. At a gradient amplitude $G = 25$ mT/m, with timing values $\delta = 30$ msec and $\Delta = 35$ msec (thus $T_E \geq 65$ msec), the gradient waveforms in Figure B8.1.1 yield $b \approx 1000$ sec/mm^2. The *b*-factor of 1000 sec/mm^2 is commonly used in clinical applications, since it provides reasonable sensitivity to diffusion contrast in the brain while maintaining good SNR. Assuming a normal brain ADC of 0.7×10^{-3} mm^2/sec, the signal reduction factor of brain in DWI at b = 1000 sec/mm^2 is exp(–0.7) or 50%. Figure B8.1.3 illustrates DW images at $b \approx 0$ (i.e., $G = 0$) and $b = 1000$. Note that the $b = 0$ image resembles standard T_2-weighted contrast (T_R =10 sec, and T_E = 73 msec), whereas the $b = 1000$ DWI exhibits the greatest signal loss in regions of high water mobility (e.g., CSF; cerebrospinal fluid). A pixel-by-pixel calculation of Equation B8.1.8 yields the ADC map shown in Figure B8.1.3C. Despite the label "apparent" diffusion coefficient, these ADC values agree with many studies of CNS (central nervous system) tissue in humans (and other species) performed on various systems at various field strengths. As expected, the ADC value of CSF is close to the diffusion coefficient of pure water at body temperature (D_{water} at 40°C = 3.1×10^{-3} mm^2/sec). Given the fact that ADC maps are reasonably quantitative suggests ADC may be useful for disease characterization across patients or serially within an individual patient.

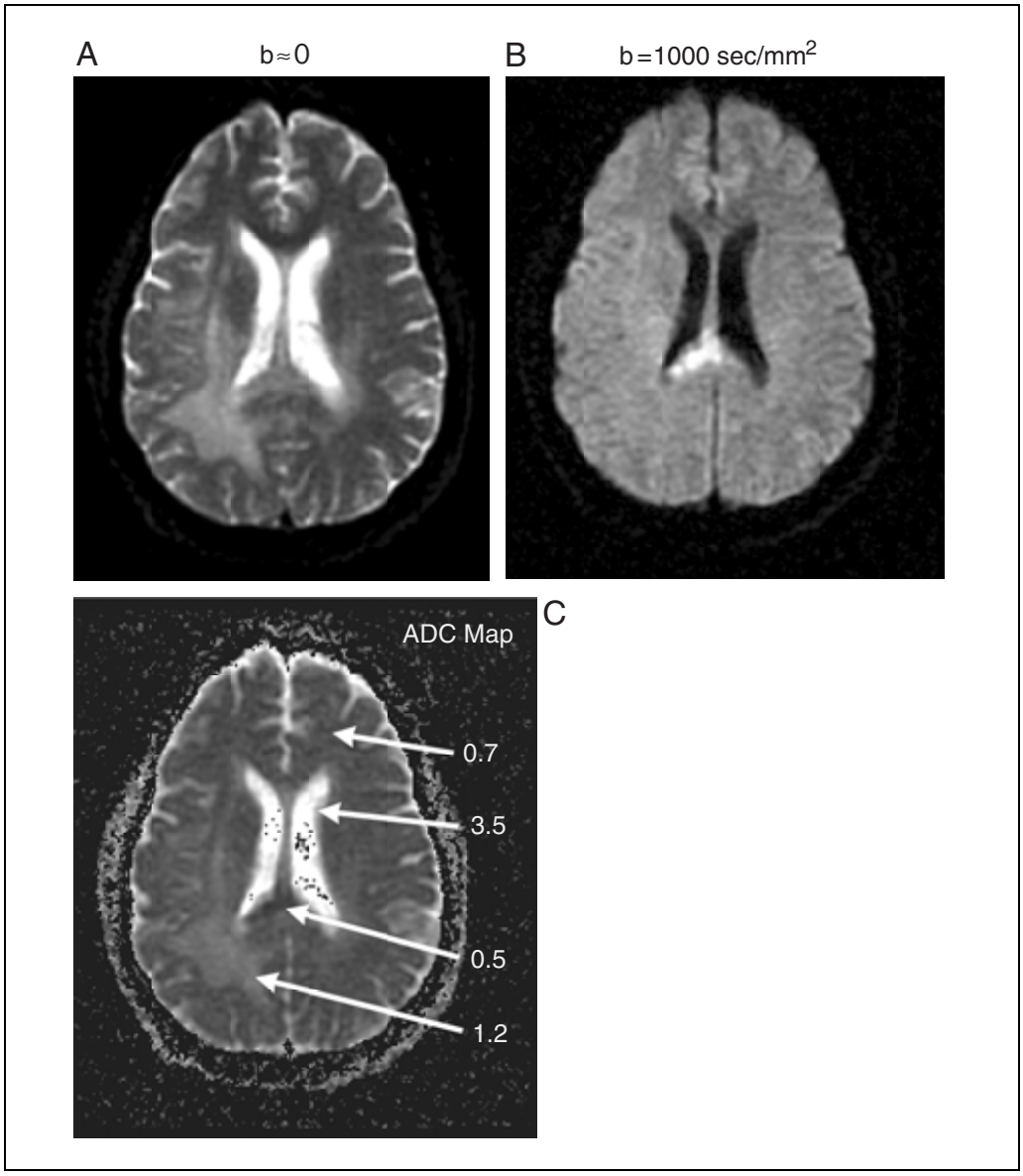

Figure B8.1.3 Diffusion-weighted images with (**A**) $b \approx 0$ and (**B**) $b = 1000$ sec/mm^2. (**C**) Calculated ADC map with ROI (region-of-interest)–derived ADC values for the indicated tissues in units of 10^{-3} mm^2/sec.

Even as qualitative images, DWI and ADC maps are routinely used in clinical practice. Heavy diffusion weighting ($b \geq 750$ sec/mm^2) in particular is recognized as a good diagnostic screen for acute stroke. As the prevalent theory goes, acute ischemia leads to cytoxic edema in which cells swell and retain excess water. The net effect of this condition is that water mobility is reduced, thus producing a bright signal on heavy DWI. Several other situations can lead to hyperintensity on DWI such as cellular-dense tissues (e.g., some tumors) and viscous environments (e.g., mucinous abscess), as well as systematic effects like coil inhomogeneity. Thus, one should keep in mind that hyperintensity on DWI does not necessarily indicate cytotoxic edema. In addition, long-T_2 tissues may have residual signal that survives diffusion weighting and thus may appear hyperintense relative to surrounding tissues—this phenomenon is referred to as "T_2 shine-through." A simple image format that removes T_2 shine-through is a noise-thresholded version of "$[S_b/S_o]$." This ratio image retains the positive aspects of DWI (namely hyperintense acute stroke lesions) while removing T_2 shine-through and coil inhomogeneity effects. The relative contrast between DWI, ADC, and $[S_b/S_o]$ ratio maps is demonstrated in Figure B8.1.4.

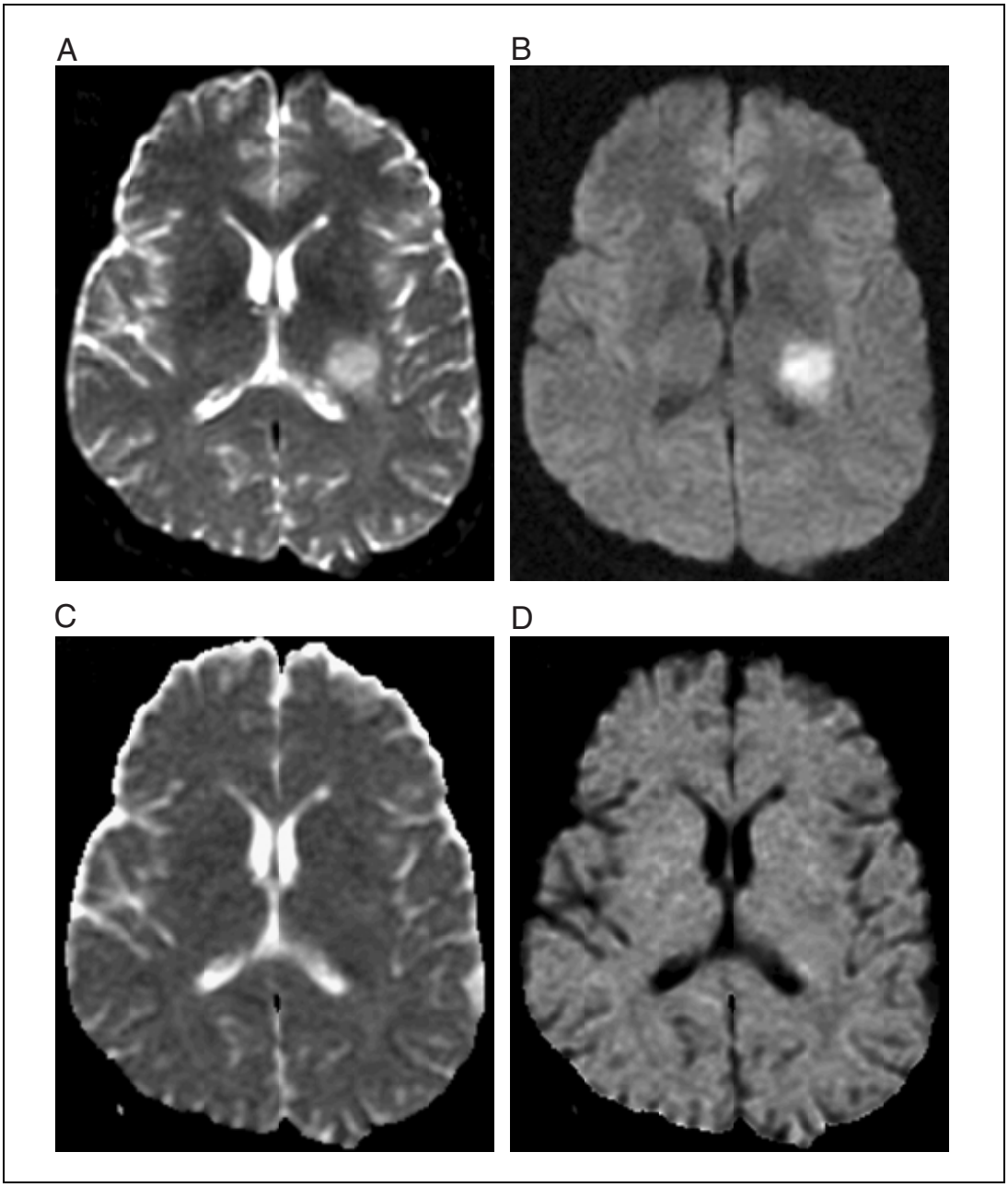

Figure B8.1.4 Comparison of contrasts between (**A**) DWI at $b \approx 0$ and (**B**) DWI at $b = 1000$ sec/mm^2; and (**C**) calculated ADC map and (**D**) ratio image [$S_b = 1000/S_b = 0$]. Note that the hyperintense lesion in (B) illustrates "T_2-shine-through" and is not due to a more restricted diffusion environment as is evident by ADC (C) and the ratio image (D).

Measures of Anisotropic Diffusion in Tissue

The next major extension to diffusion formalism relates to a potential directional dependence of water mobility. Diffusion along a particular direction in tissue will depend on directionality (if any) of structural features that impede water movement—i.e., tissues may be "anisotropic." The strongest example of diffusion anisotropy is in directionally ordered white matter structures such as the corpus callosum. Diffusion parallel to this dense band of unidirectional fibers is several fold that of diffusion perpendicular to the fibers. At this point we choose to avoid several complex mathematical issues and state without proof that for anisotropic systems the single diffusion coefficient is replaced with a 3×3 second-rank diffusion tensor:

$$\overline{\overline{D}} = \begin{bmatrix} D_{xx} & D_{xy} & D_{xz} \\ D_{xy} & D_{yy} & D_{yz} \\ D_{xz} & D_{yz} & D_{zz} \end{bmatrix} \quad \textbf{(B8.1.9)}$$

Moreover, the generalization of Equation B8.1.8 for anisotropic diffusion becomes:

$$\ln\left(\frac{S_b}{S_0}\right) = -\sum_{i=1}^{3}\sum_{j=1}^{3} b_{ij} D_{ij} \quad \textbf{(B8.1.10)}$$

where b_{ij} are elements of the "*b*-matrix," D_{ij} are elements of the symmetric diffusion tensor (see Equation B8.1.9), and subscripts *i* and *j* denote direction in the laboratory frame of reference [*x*,*y*,*z*]. The *b*-matrix is the anisotropic corollary to the isotropic *b*-factor and is calculated for each gradient condition of directionally sensitive diffusion acquisitions. More specifically, the *b*-matrix is calculated as:

$$b_{ij} = \gamma^2 \int_0^{T_E} \left(\int_0^{t'} G_i(t'')\,dt'' \right) \cdot \left(\int_0^{t'} G_j(t'')\,dt'' \right) dt' \quad \textbf{(B8.1.11)}$$

For simple gradient waveforms the *b*-matrix can be solved analytically, although because additional gradient elements are incorporated, such as used in imaging, numerical implementation of Equation B8.1.11 is preferred. At least six noncolinear diffusion gradient directions plus $b \approx 0$ are required to determine the six unique elements of the diffusion tensor in solving Equation B8.1.10 by linear regression. Note that there is a distinct *b*-matrix calculated for each DWI acquisition. A reasonable set of gradient combinations to achieve this is {[1,0,0]; [0,1,0]; [0,0,1]; [1,1,0]; [0,1,1]; and [1,0,1]} in the [*x*,*y*,*z*] laboratory frame.

Once the diffusion tensor is determined, it becomes an issue of how to efficiently summarize this information in an understandable format. Note that there are six tensor elements (D_{xx}, D_{yy}, D_{zz}, D_{xy}, D_{xz}, D_{yz}) for each pixel in the image. Certainly, grayscale images of each individual tensor element could be generated, but these would have little informational value since each represents water mobility in the laboratory frame, whereas a tissue-based frame is preferred. Also note that the preferred tissue-based frame varies with each voxel. Therefore, the following metrics are derived from the diffusion tensor for each voxel for simplified presentation in a variety of image formats.

First and foremost, it is important to maintain some measure of mobility for each voxel—i.e., an "ADC" equivalent. Fortunately, the simple average of diagonal elements of the diffusion tensor is representative of mobility for that voxel; hence, this is also often referred to as ADC. Note that there is sound mathematical justification, since this average is proportional to the trace of the diffusion tensor (trace = $D_{xx} + D_{yy} + D_{zz} = 3\text{ADC}$), which is rotationally invariant. That is, the calculated trace and ADC values are independent of the relative orientation between laboratory and tissue frames. Also, one does not need to determine the full diffusion tensor to accurately measure average mobility of an anisotropic system. That is, diffusion-weighted images acquired along any three orthogonal axes (typically [*x*,*y*,*z*] of the laboratory frame) plus $b \approx 0$ are sufficient to accurately calculate an ADC equivalent to that derived via full tensor formalism as long as the *b*-factors of the three orthogonal acquisitions are equal (i.e., $b_{xx} = b_{yy} = b_{zz}$) and off-diagonal elements of the *b*-matrix are negligible (i.e., $b_{ij} \approx 0$ for $i \neq j$). Moreover, one can directly calculate ADC from the product of these three orthogonal diffusion-weighted images as:

$$S_x = S_0 e^{-b_{xx}D_{xx}};\ S_y = S_0 e^{-b_{yy}D_{yy}};\ S_z = S_0 e^{-b_{zz}D_{zz}}$$

If $b_{xx} = b_{yy} = b_{zz} = b$

then **(B8.1.12)**

$$\text{ADC} = \frac{D_{xx} + D_{yy} + D_{zz}}{3} = \frac{1}{3b}\ln\left[\frac{S_0^3}{S_x S_y S_z}\right]$$

Of course the primary motivation for diffusion tensor imaging is to extract information relevant to directionality of tissue structures. As previously stated, the diffusion tensor is not particularly informative if left in the laboratory frame of reference. Fortunately the diffusion tensor can be converted to a tissue-based frame by rotational transformation. This mathematical operation of diagonalization is performed for each voxel and yields three non-zero diagonal elements λ_1, λ_2, λ_3, called eigenvalues, which represent the diffusivities along the three principal axes in the tissue-based frame. Using the convention $\lambda_1 \geq \lambda_2 \geq \lambda_3$, λ_1 is the principal eigenvalue representing the diffusion coefficient along the direction least restricted by structural impediments. In a unidirectional band of white matter, for example, λ_1 represents mobility parallel to the white matter fiber axis. In a purely isotropic medium such as CSF, the eigenvalues are identical. The relative orientation between laboratory and tissue-based frames are represented by unit eigenvectors, ε_i, which are also provided by the diagonalization process. The principal eigenvector corresponds to the principal eigenvalue and provides the desired directional information of fiber orientation.

Measures for the overall degree of anisotropy without regard to the direction are useful since they represent the density of unidirectionallly ordered structures. Toward that end, two very useful metrics are fractional anisotropy (FA), a measure of the portion of the magnitude of the diffusion tensor due to anisotropy:

$$\text{FA} = \sqrt{\frac{1}{2}}\frac{\sqrt{(\lambda_1 - \lambda_2)^2 + (\lambda_2 - \lambda_3)^2 (\lambda_3 - \lambda_1)^2}}{\sqrt{\lambda_1^2 + \lambda_2^2 + \lambda_3^2}} \quad \textbf{(B8.1.13)}$$

and relative anisotropy (RA), derived from a ratio of the anisotropic portion of the diffusion tensor to the isotropic portion:

$$\text{RA} = \frac{\sqrt{(\lambda_1 - \lambda_2)^2 + (\lambda_2 - \lambda_3)^2 (\lambda_3 - \lambda_1)^2}}{\lambda_1 + \lambda_2 + \lambda_3} \quad \textbf{(B8.1.14)}$$

Both anisotropy indices are dimensionless but quantitative, and acquire a value of 0.0 for a purely isotropic medium. For a highly anisotropic cylindrically symmetric medium, $\lambda_1 >> \lambda_2 = \lambda_3$. Both FA and RA maps can be presented as grayscale images for efficient visual evaluation. Finally, the volume ratio (VR) which expresses the ratio of the ellipsoid volume with axes of length λ_1, λ_2, and λ_3 (see Fig. A6.4.2) to of a sphere with radius given by the average eigenvalue, is:

$$\text{VR} = \frac{\lambda_1 \lambda_2 \lambda_3}{\left(\frac{\lambda_1 + \lambda_2 + \lambda_3}{3}\right)^3} \quad \textbf{(B8.1.15)}$$

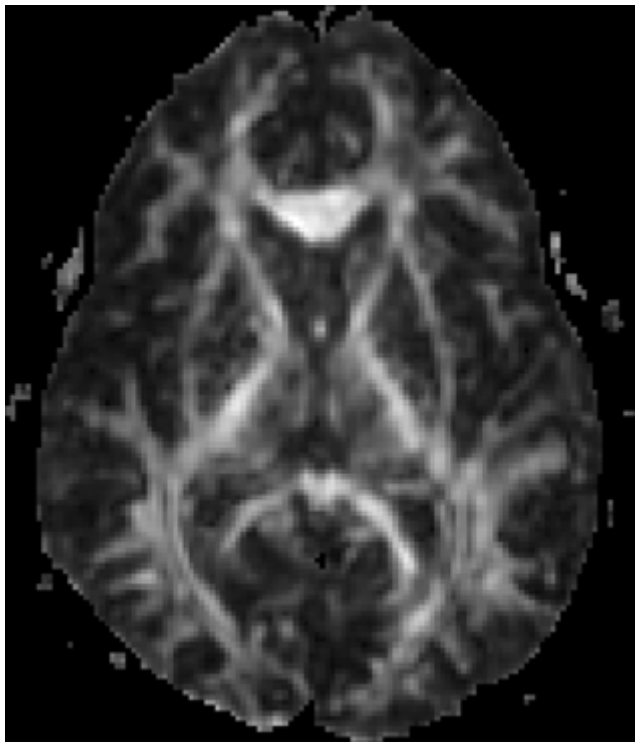

Figure B8.1.5 Representative FA map. Bright areas indicate anisotropic tissue such as white matter fiber tracts.

For purely isotropic media the behavior of the metrics is:

$$\mathrm{RA} \to 0, \mathrm{FA} \to 0, \text{ and } \mathrm{VR} \to 1$$

whereas for highly anisotropic media: **(B8.1.16)**

$$\mathrm{RA} \to \sqrt{2}, \mathrm{FA} \to 1, \text{ and } \mathrm{VR} \to 0$$

Thus, in a grayscale image, areas of brightness on RA and FA maps indicate anisotropy. To stay with this convention, sometimes it is useful to show (1 – VR) maps instead of VR, so again, brightness is an indicator of anisotropic tissue. These anisotropy maps are useful in the investigation of white-matter integrity. A representative FA map of a normal adult brain is shown in Figure B8.1.5.

An anisotropic tissue will manifest itself as bright on RA, FA, and (1 – VR) maps. What is missing from these maps is an indicator of fiber direction. It can be quite instructive to actually show the average fiber orientation in a voxel that is indicated by the eigenvector of the major eigenvalue. This information can be illustrated through the use of a whisker or quiver plot. At the position of each voxel, a small line segment is drawn indicating the projection of the major eigenvector. Additionally, the strength of the anisotropy as measured above can be used to calculate the length of the small line segments, with more anisotropy corresponding to a longer segment; little or no anisotropy is shown as a segment of vanishing length, or a point. In Figure B8.1.6A and B, we magnify the view in the region of the genu to show the fiber orientation with whiskers superimposed on anisotropy strength measured by FA.

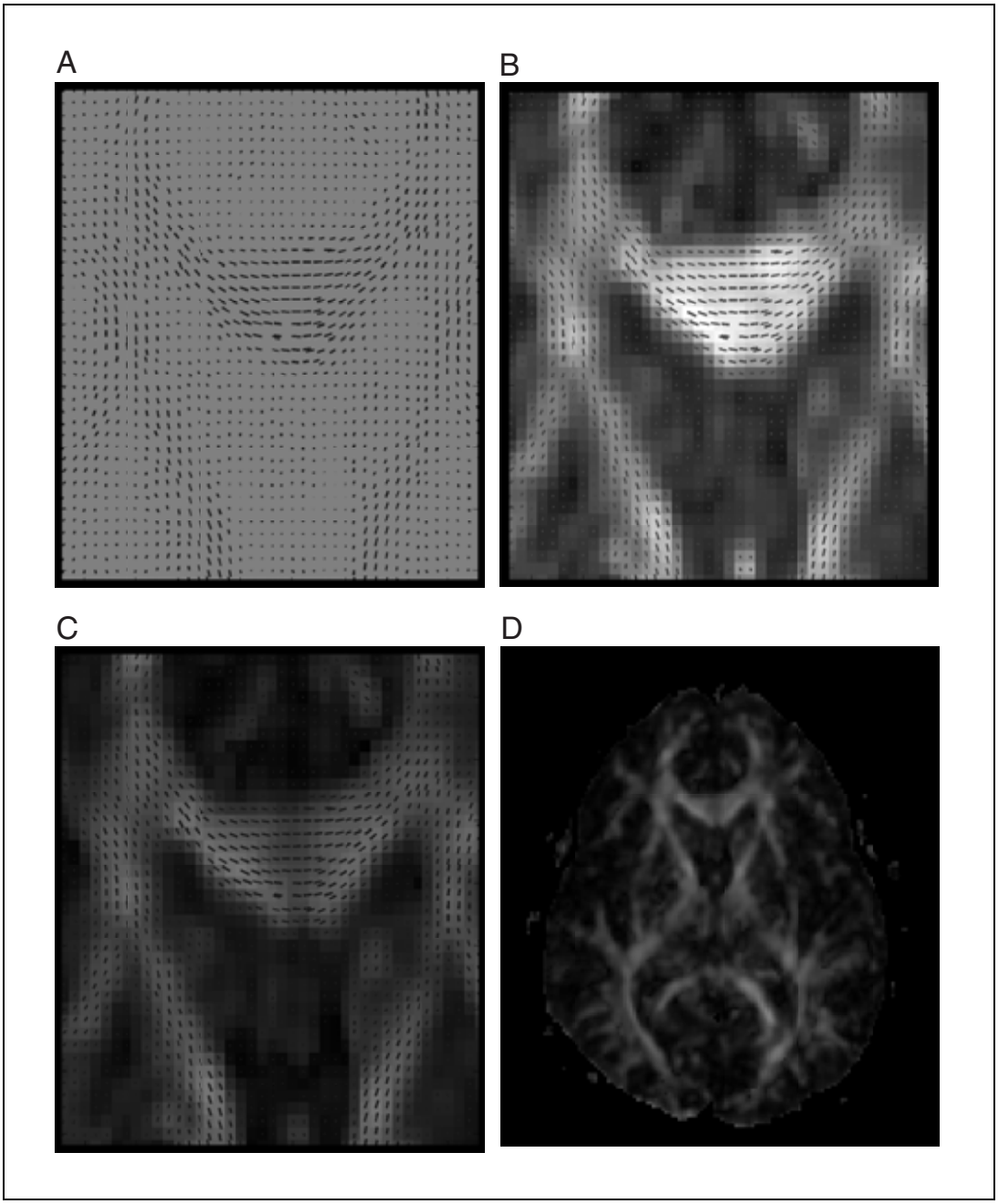

Figure B8.1.6 Expanded view of genu of the corpus callosum with line segments to indicate (**A**) projection of major eigenvectors, and (**B**) line segments superimposed on an FA map. (**C**) Color is also used to indicate right-left (red), anterior-posterior (green), and superior-inferior (blue) directions as shown in the expanded view with line-segments retained. (**D**) The full field of view image. *This black and white facsimile of the figure is intended only as a placeholder; for full-color version of figure go to http://www.interscience.wiley.com/c_p/colorfigures.htm.*

To a certain extent, these whisker maps can be quite useful, but can in themselves be slightly cumbersome to view over a large FOV. A succinct method to illustrate the direction and magnitude of anisotropy is to encode the direction of the major eigenvector in color and use a measure of the anisotropy as an illumination factor. The inferior-superior direction can be encoded in blue, left-right in red, and anterior-posterior in green as given by:

$$(R, G, B) = \mathrm{FA} \cdot \varepsilon_1 \qquad \textbf{(B8.1.17)}$$

Fibers oriented at oblique angles will now take on different hues; this results in a directionally-encoded color (DEC) fiber map. Figure B8.1.6C illustrates DEC with whiskers superimposed, and the full DEC slice is shown in Figure B8.1.6D without the augmentation of whiskers.

An elegant extension to two-dimensional whisker and/or color-coded displays is to track fiber connectivity through three-dimensional space. The majority of effort in fiber-tracking development is to improve algorithms to be robust enough to accurately follow distinct fiber tracks that inevitably coexist in voxels due to the limited spatial resolution of current image acquisition techniques. Currently, success of these algorithms is heavily dependent on SNR (signal-to-noise ratio) and resolution of the diffusion tensor images that serve as inputs to the algorithm, as well as on the use of a priori knowledge of the origination/termination of known fiber tracts. It is worth noting that fiber-tracking algorithms can produce cosmetically spectacular results with realistic-appearing fiber networks rendered in three dimensions at resolutions that defy the spatial resolution of the original DTI data. One should keep in mind that these images are somewhat synthetic and based on the model employed in the tracking algorithm—general validation of the various algorithms is still required. In fact, all DWI- and DTI-derived images are limited by the accuracy of the model on which they are based. The modest spatial resolution of DTI acquisitions suggests that a given voxel may encompass multiply oriented anisotropic domains, which violates the single-tensor model described above. Anisotropy maps, RA and FA, commonly indicate isotropic diffusion in voxels containing multiple crossing fibers due to this partial volume averaging effect.

Diffusion Imaging Sequences

Two important aspects limit the selection of imaging sequences suitable for DWI and DTI. As indicated above, at least four distinct image sets are required to estimate diffusivity (i.e., ADC) in anisotropic tissues and at least seven image sets are required for the full diffusion tensor. In practice, often, many more directions or averages are acquired to improve DTI analysis, since least-squares estimation improves with more independent directions and reduces potential bias of just a few directions. Thus, a relatively fast imaging sequence is desirable to keep DTI imaging times within reason for clinical use. In addition, the imaging sequence must be exceptionally immune to bulk tissue motion artifact. Using methods outlined in *UNIT B7.1*, the phase shift per unit motion speed is calculable for the standard bipolar gradient waveforms of Figure B8.1.1 as:

$$\left|\Phi_v\right| = \gamma G \delta \Delta. \qquad \textbf{(B8.1.18)}$$

Consider again the gradient factors previously used to achieve a *b*-factor of 1000 sec/mm^2, namely G = 25 mT/m with timing values δ = 30 msec and Δ = 35 msec. The phase shift per unit speed for this gradient is over 2π/mm/sec. That is, if conventional phase encoding schemes are used, the bulk tissue motion speed must be reproducible to well below the 0.1 mm/sec level, otherwise phase variability between phase-encoding steps would substantially degrade image quality and render ADC and tensor calculations meaningless.

The requirements for reasonably short scan times and bulk tissue motion control have made single-shot echo planar imaging (EPI) a popular choice for integration of diffusion-sensitization gradient pulses with imaging. While bulk tissue speeds in the brain can well exceed 0.1 mm/sec, the speed is relatively constant over the single-shot EPI duration to complete all phase encoding steps for a given image (≈50 msec). Good-quality diffusion-weighted EPI along three directions (plus $b = 0$) can be performed in less than a minute, with more directions and averaging as needed for DTI completed in just a few minutes. The drawbacks of single-shot EPI, such as spatial distortions due to field inhomogeneity, are well recognized and degrade DWI/DTI as well. On balance, however, single-shot EPI is the current default to perform DWI and DTI in the clinical setting. Alternatives such as phase-corrected multishot EPI or fast spin echo can improve image quality, but at the expense of longer scan times.

KEY REFERENCES

Basser, P.J. and Jones, D.K. 2002. Diffusion-tensor MRI: Theory, experimental design and data analysis—a technical review. *NMR Biomed.* 15:468-480.

An excellent review of diffusion MRI tensor mathematics and terminology.

Basser, P.J., Pajevic, S., Pierpaoli, C., Duda, J., and Aldroubi, A. 2000. In vivo fiber tractography using DT-MRI data. *Magn. Reson. Med.* 44:625-632.

Introduces fiber tracing concepts.

Le Bihan, D., Breton, E., Lallemand, D., Aubin, M.L., Vignaud, J., and Laval-Jeantet, M. 1988. Separation of diffusion and perfusion in intravoxel incoherent motion MR imaging. *Radiology*. 168:497-505.

This text is recognized as the initial clinical use of DWI.

Mori, S. and van Zijl, P.C. 2002. Fiber tracking: Principles and strategies—a technical review. *NMR Biomed.* 15:468-480.

An excellent review of fiber tracking approaches.

Moseley, M.E., Kucharczyk, J., Asgari, H.S., and Norman, D. 1991. Anisotropy in diffusion-weighted MRI. *Magn. Reson. Med.* 19:321-326.

An early demonstration of anisotropic diffusion in neural tissues in vivo.

Pierpaoli, C., Jezzard, P., Basser, P.J., Barnett, A., and Di Chiro, G. 1996. Diffusion tensor MR imaging of the human brain. *Radiology* 201:637-648.

Summarizes the initial application of diffusion tensor techniques to the normal human brain.

Stejskal, E.O. 1965. Spin diffusion measurements: Spin echoes in the presence of time-dependent field gradient. *J. Chem. Phys.* 42:288-292.

This classic article adds formalism and observation of diffusion effects in spin-echo NMR experiments.

Torrey, H. 1956. Bloch equations with diffusion terms. *Phys. Rev.* 104:563-565.

This text introduced the formalism of spin diffusion to the Bloch equations.

Contributed by Thomas L. Chenevert and Robert C. Welsh
University of Michigan
Ann Arbor, Michigan